Rapid Communications

Room-temperature skyrmions in strain-engineered FeGe thin films

Sujan Budhathoki, ¹ Arjun Sapkota, ¹ Ka Ming Law, ¹ Smriti Ranjit, ¹ Bhuwan Nepal, ¹ Brian D. Hoskins, ² Arashdeep Singh Thind, ³ Albina Y. Borisevich, ⁴ Michelle E. Jamer, ⁵ Travis J. Anderson, ⁶ Andrew D. Koehler, ⁶ Karl D. Hobart, ⁶ Gregory M. Stephen, ⁷ Don Heiman, ⁷ Tim Mewes, ¹ Rohan Mishra, ^{3,8} James C. Gallagher, ⁶ and Adam J. Hauser ¹

James C. Gallagher,⁶ and Adam J. Hauser¹

¹Department of Physics and Astronomy, University of Alabama, Tuscaloosa, Alabama 35487, USA

²Physical Measurement Laboratory, National Institute of Standards and Technology, Gaithersburg, Maryland 20899, USA

³Institute of Materials Science & Engineering, Washington University in St. Louis, One Brookings Drive, St. Louis, Missouri 63130, USA

⁴Center for Nanophase Materials Sciences, Oak Ridge National Laboratory, Oak Ridge, Tennessee 37831, USA

⁵Physics Department, United States Naval Academy, Annapolis, Maryland 21402, USA

⁶U.S. Naval Research Laboratory, Washington, DC 20375, USA

⁷Physics Department, Northeastern University, Boston, Massachusetts 02115, USA

⁸Department of Mechanical Engineering & Materials Science, Washington University in St. Louis,
One Brookings Drive, St. Louis, Missouri 63130, USA



(Received 9 March 2020; revised manuscript received 8 May 2020; accepted 12 May 2020; published 8 June 2020)

Skyrmions hold great promise for low-energy consumption and stable high-density information storage, and stabilization of the skyrmion lattice (SkX) phase at or above room temperature is greatly desired for practical use. The topological Hall effect can be used to identify candidate systems above room temperature, a challenging regime for direct observation by Lorentz electron microscopy. Atomically ordered FeGe thin films are grown epitaxially on Ge(111) substrates with \sim 4% tensile strain. Magnetic characterization reveals enhancement of the Curie temperature to 350 K due to strain, well above the bulk value of 278 K. A strong topological Hall effect was observed between 10 and 330 K, with a significant increase in magnitude observed at 330 K. The increase in magnitude occurs just below the Curie temperature, similar to the onset of the SkX phase in bulk FeGe. The results suggest that strained FeGe films may host a SkX phase above room temperature when significant tensile strain is applied.

DOI: 10.1103/PhysRevB.101.220405

Magnetic skyrmions are topologically protected magnetic spin configurations that can have a size of \sim 5 nm or less [1] and yet can be manipulated using ultralow current densities on the order of $\sim 10^6$ A/m², much less than that required for driving ferromagnetic domain walls [2-6]. These properties have attracted significant interest for spintronic applications as they could provide high information density at low power in a nonvolatile package. However, the widespread use of skyrmion technology requires new technological approaches [7] and new materials with a sufficient Curie temperature to enable the skyrmions at or just above room temperature. Skyrmions exist in either bulk chiral magnets lacking inversion symmetry or at the interface of magnetic multilayer stacks lacking mirror inversion symmetry [8–12]. Due to inversion symmetry breaking, the neighboring spins evolve at a finite angle with respect to each other to form noncollinear spin textures [3,13-16] as a result of the competition between the spin-orbit coupling-induced Dzyaloshinskii-Moriya (DM) interaction and symmetric Heisenberg exchange interaction.

Skyrmion crystal lattice (SkX) phases have been observed directly by a variety of techniques: in B20 FeGe [2] and MnSi [17] using Lorentz transmission electron microscopy (LTEM), FeCoSi [18] and Co₈Zn₈Mn₄ [19] using small-angle neutron scattering (SANS), and in Fe/Ir multilayer stacks using spin-resolved scanning tunneling microscopy (STM)

[9]. The potential for skyrmionic behavior can also be detected by topological Hall effect (THE) measurements [20,21] and ac magnetic susceptibility measurements [22]. Recently, antiskyrmions—analogous to skyrmions, but with opposite topological charge—have been demonstrated by LTEM in Heusler compounds with D_{2d} symmetry well above room temperatures [23]. Although topological Hall effect (THE) measurements are not conclusive, they have the advantage of being widespread, and unlike the previous techniques can be readily performed at room temperature without modification or concerns of thermal signal broadening.

A major obstacle to integrating skyrmions into spintronic devices is their instability in the absence of a magnetic field, since topological protection does not guarantee skyrmion stability against thermal agitation. In thin films with thicknesses less than or comparable to that of the helical wavelength, the helical ground state is suppressed, favoring skyrmion formation over a wide range of temperatures [2]. Magnetic multilayer stacks are fertile playgrounds to generate skyrmions, as they have high operating temperatures [12,24,25], but the required current density to drive skyrmions in magnetic multilayer stacks ($\sim 10^{11} \text{ A/m}^2$ [24]) is much higher than in B20 compounds ($\sim 10^6 \text{ A/m}^2$ [4,6]). In addition, magnetic multilayer stacks have a longer helical wavelength resulting in a lower skyrmion density in the SkX phase [3,26].

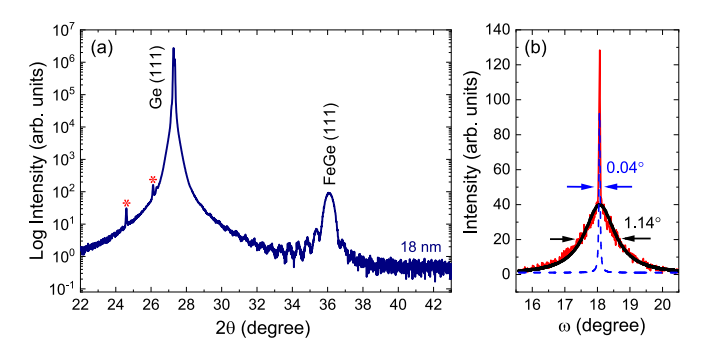


FIG. 1. (a) 2θ - ω XRD scan of an 18-nm-thick FeGe film epitaxially grown on Ge(111). Asterisks (*) indicate substrate peaks. (b) Rocking curve scan of the FeGe(111) peak showing a FWHM = 0.04° with a broad background with a FWHM = 1.14° indicative of the mosaicity spread in the crystal structure caused by lattice mismatch.

Studies have shown that the ordering temperature T_c can be tuned in B20 magnets via substrate-induced strain [27,28]. FeGe is an obvious candidate as it has the highest known $T_c \sim 278 \, \text{K}$ [2–4] within this class. In this Rapid Communication, we report the epitaxial growth of FeGe thin films on Ge(111) substrates, demonstrate strain-induced T_c enhancement, and topological Hall resistivity (THE) above the transition temperature comparable to those seen previously in SkX phases [20,27], suggesting a potential SkX formation above room temperature.

Epitaxial FeGe films of thickness 18, 72, and 102 nm were grown on Ge(111) substrates in an Ar atmosphere by sputter beam epitaxy, utilizing shuttered and beam-shaped off-axis direct-current (DC) magnetron co-sputtering of elemental Fe and Ge targets [29–31]. Films were grown with a base pressure of 6.7×10^{-7} Pa (5×10^{-9} Torr), a growth pressure of 0.7 Pa (5 mTorr), and a substrate temperature of 300° C. An Al capping layer (\sim 2.7 nm) was deposited at 100° C in order to prevent intermixing with the FeGe layer.

Energy dispersive x-ray (EDX) spectroscopy and Rutherford backscattering (RBS) determined the stoichiometry of both films in this study to be $51\% \pm 3\%$ Fe and $49\% \pm$ 3% Ge. The crystal structure, epitaxial quality, and film thickness were measured with x-ray diffraction (XRD) and x-ray reflectivity (XRR). Figure 1(a) shows the out-of-plane x-ray diffraction for an 18-nm-thick FeGe film (see Supplemental Material [32] for detailed XRD results of all three films). Pronounced Laue oscillations in the XRD patterns indicate a smooth film-substrate interface. The out-of-plane $\langle 111 \rangle d$ spacing is 2.487(2) Å, 7.9% smaller than the bulk 2.701 Å and indicative of a high tensile epitaxial strain [33–35]. Off-axis measurements show an axial distortion of the (100) peak, suggesting rhombohedral distortion due to epitaxial strain [36]. Measurements taken in the $(4\overline{10})$ and [201] directions suggest a rhombohedral angle $\alpha = 94.0^{\circ}$ and an in-plane lattice constant of 4.87(4) Å, matching the Ge substrate lattice constant of 5.658 Å with 30° in-plane rotation (4.899 Å). Although the error in estimating an in-plane lattice constant with rhombohedral distortion and mosaic twinning (see below) is significant, the above values are not found to change appreciably in the 72-nm film and so we can safely assume our film maintains the 4.1% tensile epitaxial strain indicated by the lattice mismatch.

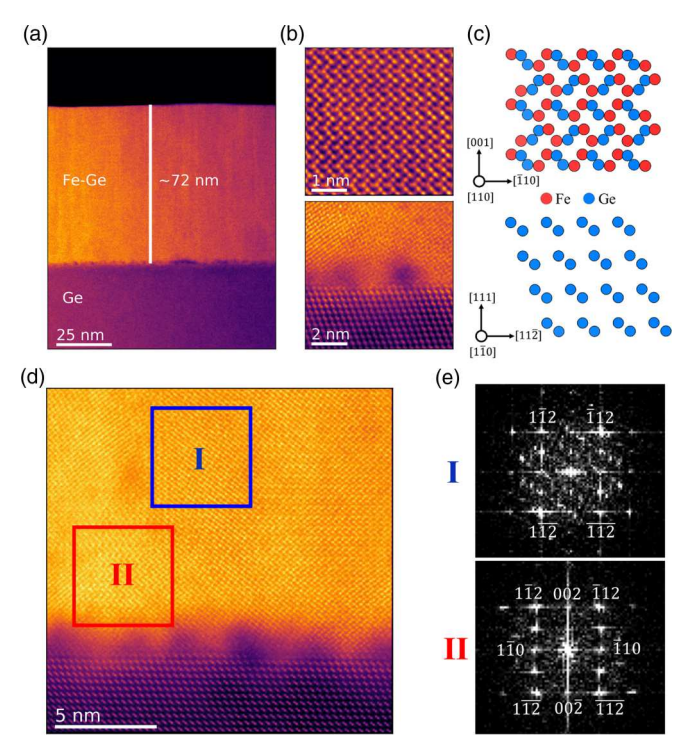


FIG. 2. (a) HAADF image showing the Ge substrate and FeGe film. (b) Atomic resolution HAADF images showing the B20 phase (top) and Ge-FeGe interface (bottom). (c) Atomic model of the B20 phase (top) and Ge with crystal orientation consistent with their respective HAADF images in (b). (d) Regions I (blue) and II (red) highlight two regions with different orientations of FeGe film. (e) Fast Fourier transform (FFT) patterns of the regions I (top) and II (bottom).

The rocking curve scan of the FeGe(111) peak is shown in Fig. 1(b). A full width at half maximum (FWHM) of 0.06° is measured, with a sharp peak (fit as a blue dashed line, FWHM 0.04°) overlaid with a broader mosaic spread peak (black solid line) likely from in-plane twinned regions in the film. This mosaic feature implies that the FeGe (111) planes are distorted within a small angular range from the substrate (111) plane to compensate for lattice mismatch while maintaining epitaxy.

The 72-nm FeGe film was imaged by aberration-corrected scanning transmission electron microscopy (STEM) (see Supplemental Material [32] for details). The atomic resolution high-angle annular dark-field (HAADF) image in Fig. 2(b) (top) shows the formation of the B20 phase, with its corresponding atomic model [37] and crystallographic orientation in Fig. 2(c) (top). Figure 2(b) (bottom) shows the Ge(111) substrate and the Ge-FeGe interface, with the corresponding crystal and orientation of the Ge(111) substrate shown in Fig. 2(c) (bottom).

We observe a \sim 1-nm-thick interfacial layer between the Ge substrate and the FeGe film, as shown in Fig. 2(b) (bottom), possibly due to imperfect epitaxy or defects left on the substrate surface during pregrowth oxide removal by HCl etch. The film also shows small regions of nonuniform crystal orientation (B20) within the film: Fig. 2(d) shows a wide field-of-view HAADF image with two regions highlighted as I (blue) and II (red). The respective fast Fourier transform

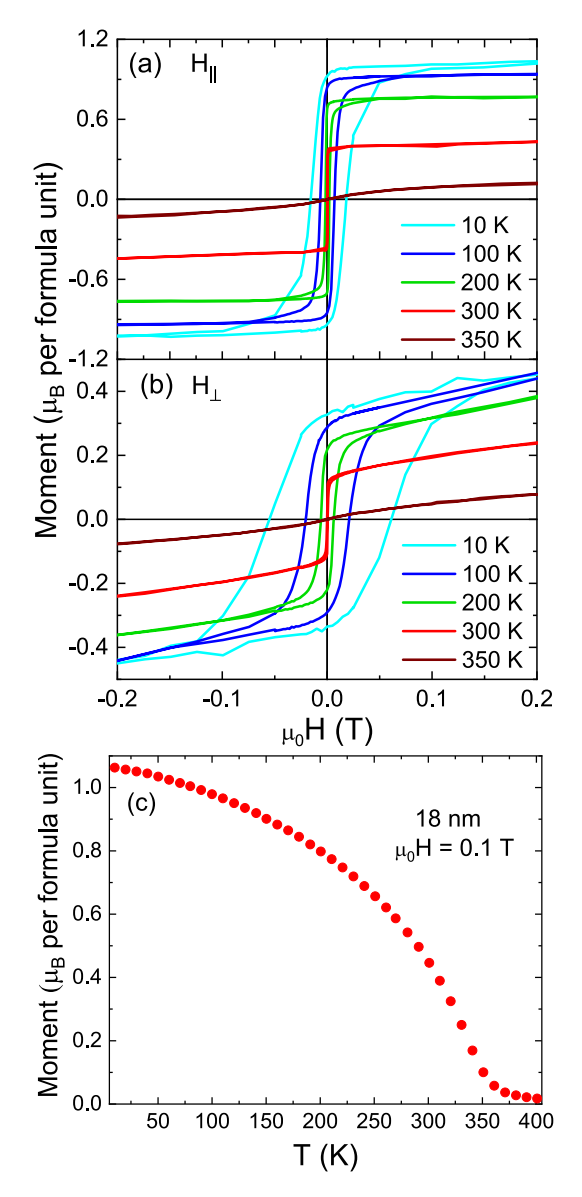


FIG. 3. SQUID data: Magnetic hysteresis loop at different temperatures for the 18 nm thick FeGe film for both in (a) in-plane (field parallel to film plane) and (b) out-of-plane (field perpendicular to film plane) configuration. (c) The temperature dependence of magnetization for the 18 nm thick FeGe film.

(FFT) patterns of regions I and II are shown in Fig. 2(e), which suggests a different crystal orientation for these two regions. The presence of small twinned volumes is corroborated semi-quantitatively by 60° offset twinning peaks in the XRD phi (ϕ) scan (see Fig. S3, Supplemental Material [32]) where the intensity of the twinned volumes is $\sim 1\%$ of that of the primary orientation peak intensities. The different crystal orientations observed in the STEM-HAADF images corroborate the twinning observed in XRD and likely explain the mosaicity spread observed in rocking curve measurements.

Magnetic properties were measured using a superconducting quantum interference device (SQUID) magnetometer. Magnetic hysteresis measurements in the in-plane and out-of-plane geometry at 10–350 K are shown in Figs. 3(a) and 3(b), respectively. We obtained a saturation magnetization

 $M_s=1.15\pm0.06\,\mu_B$ per formula unit (f.u.) at 10 K for the 18-nm-thick film. Figure 3(c) shows M as a function of T curve for the same film at an applied field of 0.1 T. The transition temperature is found to be 350 K using the Arrott plot technique [38], showing a strong Curie temperature enhancement compared to the bulk value of 278 K [2–4]. While the magnetic spins in bulk FeGe arrange themselves in a conical fashion along the body diagonal [111] crystallographic direction, strain along the body diagonal [111] decreases the distance between the nearest Fe planes, thereby increasing the strength of the exchange interaction and favoring a strong polarization of magnetic moments. Thus, more thermal energy is required to disrupt the magnetic moments and the Curie temperature is enhanced.

Broadband ferromagnetic resonance (FMR) spectroscopy was used to probe the magnetic dynamic properties of strained FeGe films at room temperature. The raw FMR signal was fitted using a Lorentzian line shape [39] in order to extract the resonance field H_{res} and peak-to-peak linewidth ΔH_{pp} . The out-of-plane H_{res} data were fitted using the Kittel formula to determine the gyromagnetic ratio γ' and effective magnetization $M_{\rm eff}$ at room temperature (RT) which were found to be 21.97 ± 0.51 GHz/T and 620 ± 9 kA/m, respectively. The observed value for γ' is lower than for typical ferromagnetic materials ($\gamma' = \frac{g\mu_B}{h} = 28 \text{ GHz/T}$ for $g \simeq 2$), and this may be attributed to the fact that the sample is not fully saturated even for the largest field in the FMR experiment (1.6 T). FMR measurements in the unsaturated regime can underestimate the value for γ' while at the same time overestimating the effective magnetization [40] for the out-of-plane configuration. If the samples are not fully saturated, then one may assume, to the first approximation, that the effective magnetization has a linear response to the applied field, which would validate the observed lower value of γ' for the out-of-plane configuration. Figure 4 also shows a nonlinear frequency dependence on H_{res} for the out-of-plane configuration at fields smaller than 1.2 T. This may be due to the noncollinear spin texture in FeGe film [28].

The effective Gilbert damping parameter $\alpha_{\rm eff}$ is determined by fitting the measured linewidths ΔH_{pp} as a linear function of the microwave frequency [41–43],

$$\Delta H(f) = \Delta H_o + \frac{2}{\sqrt{3}} \frac{\alpha_{\text{eff}}}{\nu'} f, \tag{1}$$

assuming there is no field dragging of magnetization, where f is the microwave frequency. The extrinsic linewidth for the out-of-plane configuration was determined to be $0.0251\pm0.0006\,\mathrm{T}$, less than that observed by Turgut et~al.~ [44]. Similarly, the effective damping parameter $\alpha_{\rm eff}$ was found to be 0.01 ± 0.001 , which is significantly smaller than $\alpha_{\rm eff}=0.28\pm0.02$, reported by Beg et~al.~ [45], and smaller than $\alpha_{\rm eff}=0.038\pm0.005$ at $T=258\,\mathrm{K}$, observed by Turgut et~al.~ [44] for FeGe film grown on Si(111) substrates.

Topological Hall resistivity data at a series of temperatures (10–330 K) for a field range spanning from negative to positive are shown in Fig. 5. A standard Hall bar structure was patterned from an 18-nm-thick FeGe film for electrical Hall measurements. Both the longitudinal (ρ_{xx}) and transverse Hall (ρ_{xy}) resistivity measurements were taken using a probe station at 10, 100, 290, 300, and 330 K. An electron traversing

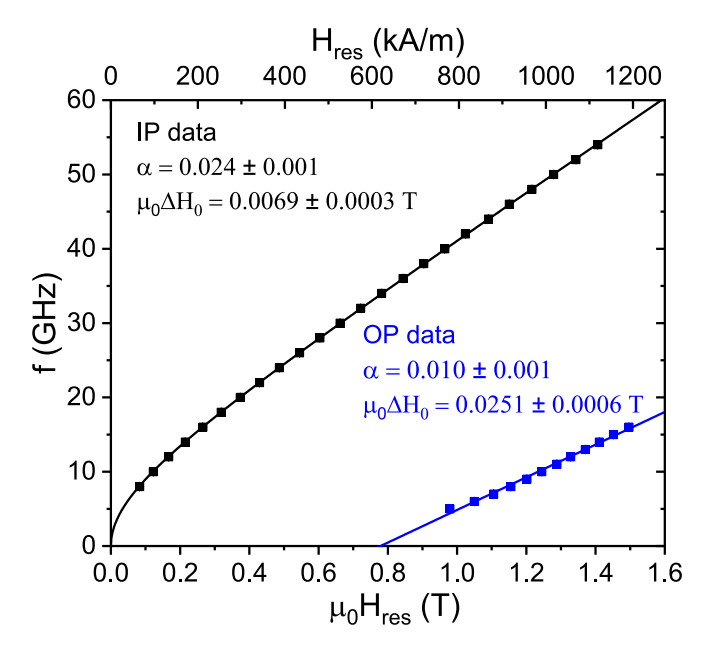


FIG. 4. Kittel plot (frequency as a function of H_{res}) at room temperature for 18-nm-thick FeGe film for both in in-plane (IP) and out-of-plane (OP) configuration.

through the skyrmionic texture follows the local magnetization profile and is deflected by the Lorentz force due to an emergent magnetic field, thus giving rise to the topological Hall effect [3,27,46–51], a signature of the skyrmionic phase [46]. The total Hall effect can be expressed as

$$\rho_{xy} = R_{OH}H_{\perp} + R_{AH}M_{\perp} + \rho_{TH}, \qquad (2)$$

where H_{\perp} is the applied magnetic field, M_{\perp} is the outof-plane magnetization, R_{OH} and R_{AH} are the ordinary and anomalous Hall coefficients, and ρ_{TH} is the topological Hall resistivity. The ordinary Hall effect scales with H, whereas the anomalous Hall effect scales with the magnetization of the sample. Two types of scattering contribute to the anomalous Hall effect: a scattering-independent mechanism ($\alpha \rho_{xx}^2$), and skew-scattering ($\beta \rho_{xx}$) mechanism caused by impurities and phonons [50]. It can be expressed as

$$R_{AH} = \alpha \rho_{xx}^2 + \beta \rho_{xx}, \tag{3}$$

where ρ_{xx} is the longitudinal resistivity. The magnetoresistance, defined as $\Delta \rho_{xx}/\rho_{xx} = [\rho_{xx}(H) - \rho_{xx}(0)]/\rho_{xx}(0)$, across all temperatures was found to be less than 0.02%, suggesting R_{AH} to be constant with applied magnetic field. The intrinsic contribution to the anomalous Hall effect depends on the details of the band structure and is largely scattering independent. The total anomalous Hall effect can be approximated to be dominated by the scattering-independent mechanism and the contribution from the skew-scattering mechanism can be ignored [52], as previously shown for FeGe thin films [20,53,54]. At fields greater than the saturation field, FeGe films are in a field-polarized state, meaning $\rho_{TH} = 0$. The total Hall resistivity can then be plotted as a function of magnetization, $R_{OH}H$ can be quantified from the intercept, and $\mu_0 R_{AH} M$ from the slope [53]. The topological Hall resistivity (ρ_{TH}) is then obtained by subtracting ordinary and anomalous Hall resistivities from the total Hall resistivity.

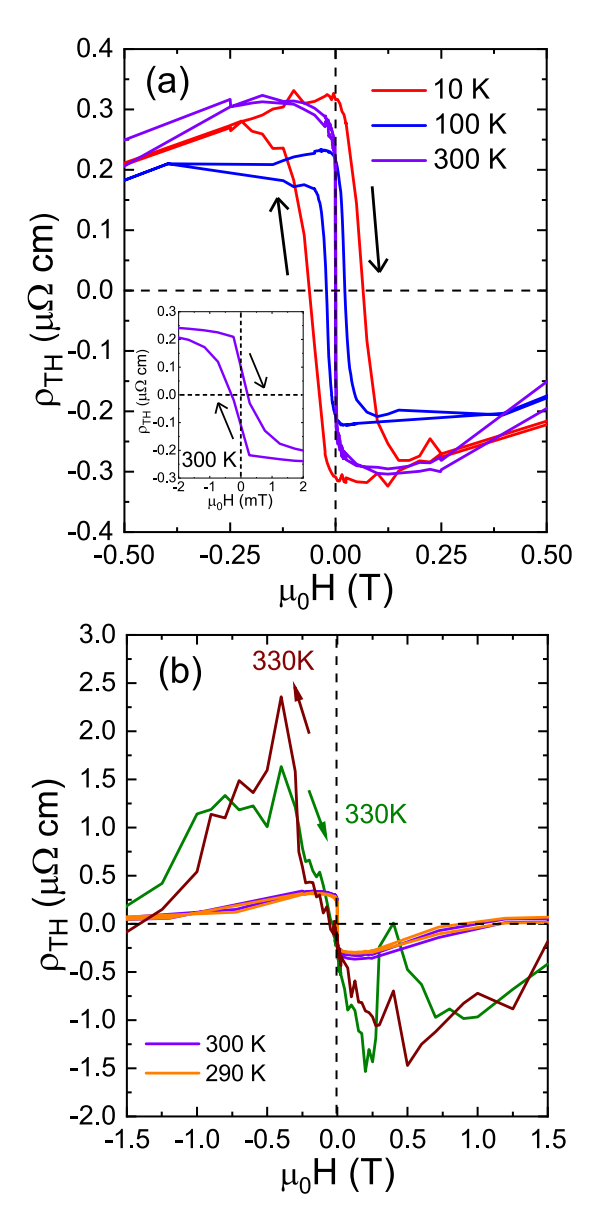


FIG. 5. The topological Hall resistivity (ρ_{TH}) hysteresis loops for the 18-nm-thick FeGe film at (a) 10, 100, and 300 K, and (b) 290, 300, and 330 K. A clear THE resistivity hysteresis loop at (a) 10, 100, and 300 K (inset) is the indicative of a noncollinear phase.

As shown in Fig. 5, the 18-nm-film exhibits clear topological Hall resistivity hysteresis loops with strong nonzero ρ_{TH} values at zero fields up to 300 K, demonstrating a noncollinear phase up to RT. A significant topological Hall effect ($\rho_{TH}=326~\text{n}\Omega\,\text{cm}$) is observed at 10 K, which gradually decreases up to 290 K and then sharply increases ($\rho_{TH}=2.34~\mu\Omega\,\text{cm}$) at 330 K. This temperature, relative to T_c , is consistent with the temperature range expected for skyrmion lattice formation in bulk FeGe and B20 magnets in general [6,20]. This observed ρ_{TH} value at 330 K is significantly larger than in metallic multilayers [25] and in unstrained FeGe thin films [20]. Significant directional dependence for the maximum ρ_{TH} is observed at 330 K at ± 0.4 T when the field is scanned from positive (negative) to negative (positive). It should be noted that competing magnetic phases

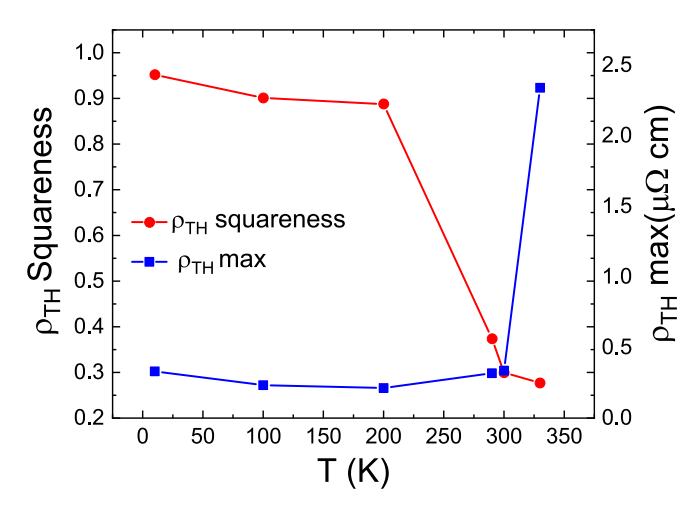


FIG. 6. The squareness of the topological Hall resistivity (ρ_{TH}) for a corresponding maximum value of (ρ_{TH}) for the 18-nm FeGe film between 10 and 330 K.

(e.g., helical and conical) can persist at the low-temperature regime. These phases can potentially contribute to the topological Hall resistivity and cannot be excluded completely. As shown in Fig. 6, the maximum value of ρ_{TH} remains relatively constant close to RT and then suddenly spikes above RT, whereas the squareness $[\rho_{TH}(H=0)/\rho_{TH}(max)]$ of ρ_{TH} plummets above 200 K, suggesting a possible metastable SkX phase.

The topological Hall effect is frequently attributed as a signature of the magnetic spin texture and the observed Hall anomaly close to T_c reminiscent of the skyrmion lattice phase. However, it is worth recalling that other mechanisms have been either theorized or observed to contribute to the total Hall effect in chiral magnets with perpendicular magnetic anisotropy, e.g., thermal fluctuations of topological excitations [55,56]. However, the magnitude of the observed THE in our film is much larger and so can probably be ruled out

as this thermal effect. The increased noise level at 330 K at lower fields departing from the field-polarized state can be attributed to the low current needed to measure the Hall data on a film on a narrow-band-gap Ge substrate at elevated temperatures without exceeding 2% leakage current during the measurement. Attempts to perform LTEM at elevated temperatures have been unsuccessful as data acquisition is greatly affected above room temperature. Small-angle neutron scattering is proposed to resolve this issue and corroborate skyrmion formation in strained FeGe thin films.

In conclusion, we have grown phase-pure epitaxial FeGe films on a Ge(111) substrate with coherent \sim 4% tensile strain, and demonstrate strain-induced T_c enhancement well above room temperature while preserving the B20 crystal structure, albeit with slight structural distortions. A small value for the effective Gilbert damping parameter is measured compared to previous reports, critical for potential application in spintronics. Additionally, significant ρ_{TH} at zero field is observed in a wide temperature window from 10 to 330 K and a strong $\rho_{TH} = 2.34~\mu\Omega$ cm at 330 K close to observed T_c with distinct TH peaks at \pm 0.4 T. These features can be attributed to the emergent magnetic field caused by the noncollinear spin arrangement and suggest a potential skyrmion formation above room temperature.

Support is acknowledged from the following National Science Foundation grants: NSF-CAREER Grants No. 1452670 (A.S.); No. DMR-1806147 (A.S.T. and R.M.); No. DMR-1904446 (M.E.J.); and No. DMR-1905662 (D.H). Support is acknowledged from NASA Grant NASA CAN80NSSC18M0023 (T.M.). The authors (T.J.A, A.D.K., K.D.H., and J.C.G.) would like to acknowledge the Office of Naval Research. Aberration-corrected STEM experiments were conducted at the Center for Nanophase Materials Sciences at Oak Ridge National Laboratory, which is a US Department of Energy (DOE) Office of Science User Facility, through a user project.

^[1] X. Wang, H. Yuan, and X. Wang, A theory on skyrmion size, Commun. Phys. 1, 1 (2018).

^[2] X. Yu, N. Kanazawa, Y. Onose, K. Kimoto, W. Zhang, S. Ishiwata, Y. Matsui, and Y. Tokura, Near room-temperature formation of a skyrmion crystal in thin-films of the helimagnet FeGe, Nat. Mater. 10, 106 (2011).

^[3] N. Nagaosa and Y. Tokura, Topological properties and dynamics of magnetic skyrmions, Nat. Nanotechnol. **8**, 899 (2013).

^[4] X. Yu, N. Kanazawa, W. Zhang, T. Nagai, T. Hara, K. Kimoto, Y. Matsui, Y. Onose, and Y. Tokura, Skyrmion flow near room temperature in an ultralow current density, Nat. Commun. 3, 988 (2012).

^[5] A. Fert, V. Cros, and J. Sampaio, Skyrmions on the track, Nat. Nanotechnol. 8, 152 (2013).

^[6] F. Jonietz, S. Mühlbauer, C. Pfleiderer, A. Neubauer, W. Münzer, A. Bauer, T. Adams, R. Georgii, P. Böni, R. A. Duine *et al.*, Spin transfer torques in MnSi at ultralow current densities, Science 330, 1648 (2010).

^[7] R. Cheng, M. Li, A. Sapkota, A. Rai, A. Pokhrel, T. Mewes, C. Mewes, D. Xiao, M. De Graef, and V. Sokalski, Magnetic domain wall skyrmions, Phys. Rev. B 99, 184412 (2019).

^[8] A. Fert, N. Reyren, and V. Cros, Magnetic skyrmions: Advances in physics and potential applications, Nat. Rev. Mater. 2, 17031 (2017).

^[9] S. Heinze, K. Von Bergmann, M. Menzel, J. Brede, A. Kubetzka, R. Wiesendanger, G. Bihlmayer, and S. Blügel, Spontaneous atomic-scale magnetic skyrmion lattice in two dimensions, Nat. Phys. 7, 713 (2011).

^[10] N. Romming, C. Hanneken, M. Menzel, J. E. Bickel, B. Wolter, K. von Bergmann, A. Kubetzka, and R. Wiesendanger, Writing and deleting single magnetic skyrmions, Science 341, 636 (2013).

^[11] G. Chen, T. Ma, A. T. N'Diaye, H. Kwon, C. Won, Y. Wu, and A. K. Schmid, Tailoring the chirality of magnetic domain walls by interface engineering, Nat. Commun. 4, 2671 (2013).

- [12] C. Moreau-Luchaire, C. Moutafis, N. Reyren, J. Sampaio, C. Vaz, N. Van Horne, K. Bouzehouane, K. Garcia, C. Deranlot, P. Warnicke *et al.*, Additive interfacial chiral interaction in multilayers for stabilization of small individual skyrmions at room temperature, Nat. Nanotechnol. 11, 444 (2016).
- [13] I. Dzyaloshinsky, A thermodynamic theory of "weak" ferromagnetism of antiferromagnetics, J. Phys. Chem. Solids 4, 241 (1958).
- [14] T. Moriya, Anisotropic superexchange interaction and weak ferromagnetism, Phys. Rev. 120, 91 (1960).
- [15] B. Binz and A. Vishwanath, Theory of helical spin crystals: Phases, textures, and properties, Phys. Rev. B 74, 214408 (2006).
- [16] J. H. Han, J. Zang, Z. Yang, J.-H. Park, and N. Nagaosa, Skyrmion lattice in a two-dimensional chiral magnet, Phys. Rev. B 82, 094429 (2010).
- [17] S. Mühlbauer, B. Binz, F. Jonietz, C. Pfleiderer, A. Rosch, A. Neubauer, R. Georgii, and P. Böni, Skyrmion lattice in a chiral magnet, Science 323, 915 (2009).
- [18] X. Yu, Y. Onose, N. Kanazawa, J. Park, J. Han, Y. Matsui, N. Nagaosa, and Y. Tokura, Real-space observation of a two-dimensional skyrmion crystal, Nature (London) 465, 901 (2010).
- [19] K. Karube, J. White, N. Reynolds, J. Gavilano, H. Oike, A. Kikkawa, F. Kagawa, Y. Tokunaga, H. M. Rønnow, Y. Tokura *et al.*, Robust metastable skyrmions and their triangular– square lattice structural transition in a high-temperature chiral magnet, Nat. Mater. 15, 1237 (2016).
- [20] J. C. Gallagher, K. Y. Meng, J. T. Brangham, H. L. Wang, B. D. Esser, D. W. McComb, and F. Y. Yang, Robust Zero-Field Skyrmion Formation in FeGe Epitaxial Thin Films, Phys. Rev. Lett. 118, 027201 (2017).
- [21] H. Oike, A. Kikkawa, N. Kanazawa, Y. Taguchi, M. Kawasaki, Y. Tokura, and F. Kagawa, Interplay between topological and thermodynamic stability in a metastable magnetic skyrmion lattice, Nat. Phys. 12, 62 (2016).
- [22] H. Wilhelm, M. Baenitz, M. Schmidt, U. K. Rößler, A. A. Leonov, and A. N. Bogdanov, Precursor Phenomena at the Magnetic Ordering of the Cubic Helimagnet FeGe, Phys. Rev. Lett. 107, 127203 (2011).
- [23] A. K. Nayak, V. Kumar, T. Ma, P. Werner, E. Pippel, R. Sahoo, F. Damay, U. K. Rößler, C. Felser, and S. S. Parkin, Magnetic antiskyrmions above room temperature in tetragonal Heusler materials, Nature (London) 548, 561 (2017).
- [24] S. Woo, K. Litzius, B. Krüger, M.-Y. Im, L. Caretta, K. Richter, M. Mann, A. Krone, R. M. Reeve, M. Weigand *et al.*, Observation of room-temperature magnetic skyrmions and their current-driven dynamics in ultrathin metallic ferromagnets, Nat. Mater. 15, 501 (2016).
- [25] A. Soumyanarayanan, M. Raju, A. G. Oyarce, A. K. Tan, M.-Y. Im, A. P. Petrović, P. Ho, K. Khoo, M. Tran, C. Gan *et al.*, Tunable room-temperature magnetic skyrmions in Ir/Fe/Co/Pt multilayers, Nat. Mater. 16, 898 (2017).
- [26] D. Maccariello, W. Legrand, N. Reyren, K. Garcia, K. Bouzehouane, S. Collin, V. Cros, and A. Fert, Electrical detection of single magnetic skyrmions in metallic multilayers at room temperature, Nat. Nanotechnol. 13, 233 (2018).
- [27] Y. Li, N. Kanazawa, X. Z. Yu, A. Tsukazaki, M. Kawasaki, M. Ichikawa, X. F. Jin, F. Kagawa, and Y. Tokura, Robust

- Formation of Skyrmions and Topological Hall Effect Anomaly in Epitaxial Thin Films of MnSi, Phys. Rev. Lett. **110**, 117202 (2013).
- [28] S. Zhang, I. Stasinopoulos, T. Lancaster, F. Xiao, A. Bauer, F. Rucker, A. Baker, A. Figueroa, Z. Salman, F. Pratt *et al.*, Room-temperature helimagnetism in FeGe thin films, Sci. Rep. 7, 123 (2017).
- [29] A. J. Hauser, R. E. A. Williams, R. A. Ricciardo, A. Genc, M. Dixit, J. M. Lucy, P. M. Woodward, H. L. Fraser, and F. Yang, Unlocking the potential of half-metallic Sr₂FeMoO₆ films through controlled stoichiometry and double-perovskite ordering, Phys. Rev. B 83, 014407 (2011).
- [30] B. Peters, A. Alfonsov, C. Blum, S. J. Hageman, P. Woodward, S. Wurmehl, B. Büchner, and F. Yang, Epitaxial films of Heusler compound Co₂FeAl_{0.5}Si_{0.5} with high crystalline quality grown by off-axis sputtering, Appl. Phys. Lett. 103, 162404 (2013).
- [31] S. Budhathoki, A. Sapkota, K. M. Law, B. Nepal, S. Ranjit, K. Shambhu, T. Mewes, and A. J. Hauser, Low Gilbert damping and linewidth in magnetostrictive FeGa thin films, J. Magn. Magn. Mater. 496, 165906 (2020).
- [32] See Supplemental Material at http://link.aps.org/supplemental/ 10.1103/PhysRevB.101.220405 for additional information on film growth, sample preparation for STEM, 2θ - ω XRD, XRR and ϕ -scans of the FeGe films, FMR data and the analysis to extract topological Hall resistivity.
- [33] H. Wilhelm, M. Schmidt, R. Cardoso-Gil, U. Burkhardt, M. Hanfland, U. Schwarz, and L. Akselrud, Structural investigations of ε-FeGe at high pressure and low temperature, Sci. Technol. Adv. Mater. 8, 416 (2007).
- [34] P. Pedrazzini, H. Wilhelm, D. Jaccard, T. Jarlborg, M. Schmidt, M. Hanfland, L. Akselrud, H. Q. Yuan, U. Schwarz, Yu. Grin, and F. Steglich, Metallic State in Cubic FeGe Beyond its Quantum Phase Transition, Phys. Rev. Lett. 98, 047204 (2007).
- [35] B. Lebech, J. Bernhard, and T. Freltoft, Magnetic structures of cubic FeGe studied by small-angle neutron scattering, J. Phys.: Condens. Matter 1, 6105 (1989).
- [36] M. De Graef and M. E. McHenry, Structure of Materials: An Introduction to Crystallography, Diffraction and Symmetry (Cambridge University Press, Cambridge, UK, 2012).
- [37] M. Richardson, Crystal structure refinements of the B20 and monoclinic (CoGe-type) polymorphs of FeGe, Acta Chem. Scand. 21, 753 (1967).
- [38] A. Arrott and J. E. Noakes, Approximate Equation of State For Nickel Near its Critical Temperature, Phys. Rev. Lett. 19, 786 (1967).
- [39] C. Oates, F. Ogrin, S. Lee, P. Riedi, G. Smith, and T. Thomson, High field ferromagnetic resonance measurements of the anisotropy field of longitudinal recording thin-film media, J. Appl. Phys. 91, 1417 (2002).
- [40] B. Khodadadi, J. B. Mohammadi, C. Mewes, T. Mewes, M. Manno, C. Leighton, and C. W. Miller, Enhanced spin pumping near a magnetic ordering transition, Phys. Rev. B 96, 054436 (2017).
- [41] C. K. Mewes and T. Mewes, Relaxation in magnetic materials for spintronics, in *Handbook of Nanomagnetism: Applications* and *Tools*, edited by R. A. Lukaszew (Jenny Stanford Publishing, New York, 2015), p. 71.

- [42] B. Heinrich, J. Cochran, and R. Hasegawa, FMR linebroadening in metals due to two-magnon scattering, J. Appl. Phys. 57, 3690 (1985).
- [43] R. D. McMichael, D. J. Twisselmann, and A. Kunz, Localized Ferromagnetic Resonance in Inhomogeneous Thin Films, Phys. Rev. Lett. 90, 227601 (2003).
- [44] E. Turgut, A. Park, K. Nguyen, A. Moehle, D. A. Muller, and G. D. Fuchs, Chiral magnetic excitations in FeGe films, Phys. Rev. B 95, 134416 (2017).
- [45] M. Beg, M. Albert, M.-A. Bisotti, D. Cortés-Ortuño, W. Wang, R. Carey, M. Vousden, O. Hovorka, C. Ciccarelli, C. S. Spencer, C. H. Marrows, and H. Fangohr, Dynamics of skyrmionic states in confined helimagnetic nanostructures, Phys. Rev. B 95, 014433 (2017).
- [46] A. Neubauer, C. Pfleiderer, B. Binz, A. Rosch, R. Ritz, P. G. Niklowitz, and P. Böni, Topological Hall Effect in the A Phase of MnSi, Phys. Rev. Lett. 102, 186602 (2009).
- [47] N. Kanazawa, Y. Onose, T. Arima, D. Okuyama, K. Ohoyama, S. Wakimoto, K. Kakurai, S. Ishiwata, and Y. Tokura, Large Topological Hall Effect in a Short-Period Helimagnet MnGe, Phys. Rev. Lett. 106, 156603 (2011).
- [48] J. Zang, M. Mostovoy, J. H. Han, and N. Nagaosa, Dynamics of Skyrmion Crystals in Metallic Thin Films, Phys. Rev. Lett. 107, 136804 (2011).

- [49] T. Schulz, R. Ritz, A. Bauer, M. Halder, M. Wagner, C. Franz, C. Pfleiderer, K. Everschor, M. Garst, and A. Rosch, Emergent electrodynamics of skyrmions in a chiral magnet, Nat. Phys. 8, 301 (2012).
- [50] N. Nagaosa, J. Sinova, S. Onoda, A. H. MacDonald, and N. P. Ong, Anomalous Hall effect, Rev. Mod. Phys. 82, 1539 (2010).
- [51] C. Pfleiderer and A. Rosch, Condensed-matter physics: Single skyrmions spotted, Nature (London) 465, 880 (2010).
- [52] E. Y. Tsymbal and I. Zutic, Handbook of Spin Transport and Magnetism (CRC Press, Boca Raton, FL, 2011).
- [53] S. X. Huang and C. L. Chien, Extended Skyrmion Phase in Epitaxial FeGe(111) Thin Films, Phys. Rev. Lett. 108, 267201 (2012).
- [54] N. A. Porter, J. C. Gartside, and C. H. Marrows, Scattering mechanisms in textured FeGe thin films: Magnetoresistance and the anomalous Hall effect, Phys. Rev. B 90, 024403 (2014).
- [55] W.-T. Hou, J.-X. Yu, M. Daly, and J. Zang, Thermally driven topology in chiral magnets, Phys. Rev. B **96**, 140403(R) (2017).
- [56] W. Wang, M. W. Daniels, Z. Liao, Y. Zhao, J. Wang, G. Koster, G. Rijnders, C.-Z. Chang, D. Xiao, and W. Wu, Spin chirality fluctuation in two-dimensional ferromagnets with perpendicular magnetic anisotropy, Nat. Mater. 18, 1054 (2019).